Journal of Materials Chemistry A

Presentation of Gas-phase-reactant-accessible Single-rhodium-atom Catalysts for CO Oxidation, via MOF Confinement of an Anderson Polyoxometalate

Journal:	*Journal of Materials Chemistry A*
Manuscript ID	TA-ART-05-2022-003975.R1
Article Type:	Paper
Date Submitted by the Author:	20-Jul-2022
Complete List of Authors:	Liu, Qin; University of Science and Technology of China School of Chemistry and Materials Science, Chen, Zhihengyu; Stony Brook University, Chemistry Shabbir, Hafeera; Clemson University, Chemical and Biomolecular Engineering Duan, Jiaxin; Northwestern University Bi, Wentuan; University of Science and Technology of China, Hefei National Laboratory for Physical Sciences at Microscale; University of Science and Technology of China, Department of Chemistry Lu, Zhiyong; Hohai University, College of Mechanics and Materials; Nanjing University, State Key Laboratory of Coordination Chemistry, School of Chemistry and Chemical Engineering Schweitzer, Neil; Northwestern University, Center for Catalysis and Surface Science; Argonne National Laboratory, Chemical Science and Engineering Division Alayoglu, Selim; Northwestern University Goswami, Subhadip; Northwestern University, Chemistry Chapman, Karena; Stony Brook University, Chemistry Getman, Rachel; Clemson University, Chemical and Biomolecular Engineering Wang, Qining ; Northwestern University Notestein, Justin; Northwestern University, Chemical and Biological Engineering Hupp, Joseph; Northwestern University, Department of Chemistry

ARTICLE

Presentation of Gas-phase-reactant-accessible Single-rhodium-atom Catalysts for CO Oxidation, via MOF Confinement of an Anderson Polyoxometalate

Received 00th January 20xx,
Accepted 00th January 20xx

DOI: 10.1039/x0xx00000x

Qin Liu,*[a,b] Zhihengyu Chen,[c] Hafeera Shabbir,[d] Jiaxin (Dawn) Duan,[b] Wentuan Bi,[a,b] Zhiyong Lu,[b,e] Neil Schweitzer,[f] Selim Alayoglu,[f] Subhadip Goswami,[b] Karena W. Chapman,[c] Rachel B Getman,[d] Qining Wang,[b] Justin M. Notestein,[b] and Joseph T. Hupp*[b]

Geometric or electronic confinement of guests within nanoporous hosts holds promise for imparting catalytic functionality, including single-metal-atom catalytic functionality, to existing materials. When the nanoporous host is a metal-organic framework (MOF), single-metal-ion catalysts have typically been installed by grafting to an open site on an inorganic node, with the node effectively becoming the support for the catalyst. This approach, however, imposes compositional constraints, as the node not only needs to be receptive to grafting, but also must be capable of stabilizing the framework against solvent evacuation, chemical exposure, and heating. Here, we show that disk-like, Anderson polyoxometalate clusters ($RhMo_6O_{24}^{n-}$ and $Mo_7O_{24}^{m-}$; POMs) can be confined in pore-specific and orientation-specific fashion within the hierarchically porous, Zr(IV)-based MOF, NU1K. Self-limiting loading of one cluster per pore, and associated nano-confinement, serve to isolate each POM and prevent consolidation caused by sintering. Additionally, the oriented confinement serves to expose individual rhodium atoms to candidate gas-phase reactants, while enabling the rhodium atom to employ a well-defined oxy-molybdenum cluster, rather than a MOF node, as a support. Synchrotron-based difference-electron-density maps and differential pair-distribution-function analyses of scattered X-rays establish cluster siting and orientation and confirm isolation. Nanoconfined (*i.e.*, MOF- and POM-confined) single-rhodium(III)-atoms are catalytically competent for an illustrative gas-phase reaction, CO oxidation by O_2, with the MOF-isolated POM enormously outperforming nonporous, MOF-free, solid $(NH_4)_3[H_6RhMo_6O_{24}]\cdot 6H_2O$. This work highlights the value of MOF-based nano-confinement and oriented isolation of planar POMs as a means of uniformly presenting and stabilizing potent single-metal-atom catalysts, in reactant-accessible form, on well-defined supports.

Introduction

In view of their inherent simplicity, single-atom-catalysts[1] (also termed "atomically dispersed supported metal catalysts") present exciting opportunities for advancing our understanding of Catalysis Science,[2] especially in the context heterogeneous catalysis of gas-phase chemical transformations and condensed-phase electrochemical reactions. Among the more widely explored approaches to single-atom-catalyst presentation, especially in sinter-resistant form, are methods centering on: a) dilute, nanoparticulate metal alloys,[3] b) pyrolysis-derived metal-ion coordination within the exposed planes of nitrogen-doped, high-area graphite,[4] and c) grafting of metal ions to organic-linker-separated, inorganic nodes (typically oxy-metal clusters) of porous metal-organic framework (MOF) compounds.[5-9] While all are effective, each can at times present challenges with respect to active-site characterization, catalyst-uniformity, or catalyst-stability. Herein, we describe a complementary approach that, in favorable cases, can help circumvent these challenges. By way of illustration, we show that disk-like, Anderson polyoxometalate (POM) clusters[10] can be confined in pore-specific and orientation-specific fashion within a MOF offering size-matched micropores, together with pores of larger size that can facilitate molecular transport of reactants and products. The installed single-metal-atoms inhabit identical coordination environments, resist agglomeration, and display sustained

[a] School of Chemistry and Materials Science, University of Science and Technology of China, Hefei 230026, China.
[b] Department of Chemistry, Northwestern University, Evanston, Illinois 60208, USA.
[c] Department of Chemistry, Stony Brook University, New York 11794-3400, USA
[d] Chemical and Biomolecular Engineering, Clemson University, Clemson, SC 29634, USA
[e] College of Mechanics and Materials, Hohai University, Nanjing 210098, China.
[f] Department of Chemical and Biological Engineering, Center for Catalysis and Surface Science, Northwestern University, Evanston, Illinois 60208-3113, USA
† E-mail id- *qin0623@ustc.edu.cn,
*j-hupp@northwestern.edu.

Electronic Supplementary Information (ESI) available: instrumentation, additional characterization (FTIR, SEM, EDS mapping, NMR, XPS, PDF, DRITFS, DED, dPDF, PXRD, gravimetric isotherm and gravimetric pore size distribution, crystal data), analysis of activation energy, XAFS, computational modeling of structure that reproduces experimental DRIFT spectrum, computational modeling of catalytic form of structure of MOF-installed Rh-containing POM. See DOI: 10.1039/x0xx00000x

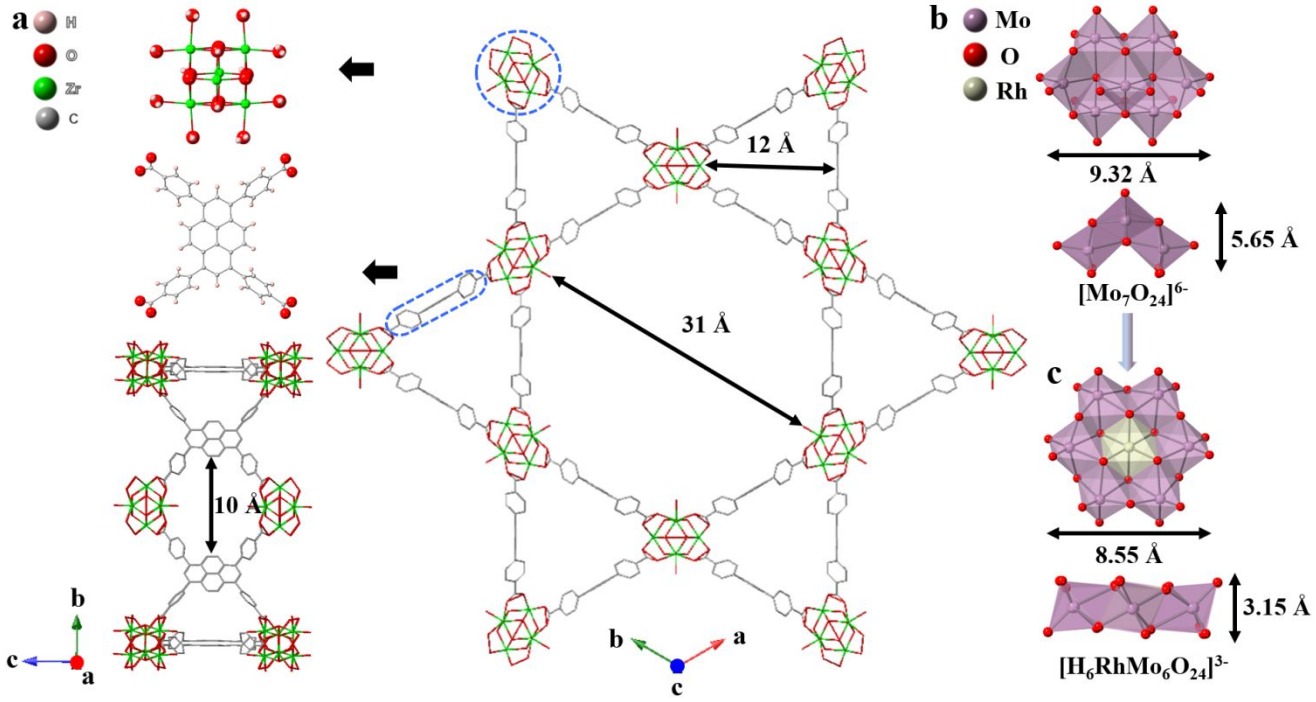

Figure 1. (a) Crystal structure of NU1K, showing the mesoporous (31 Å) and microporous (12 Å) channels. Each layer is separated by 10 Å windows. The channels are interconnected with each other through the 8 × 10 Å windows (*c*-pores). The structures for the nodes and linkers are given. Polyhedral representation and size of (b) $[Mo_7O_{24}]^{6-}$ and (c) $[H_6RhMo_6O_{24}]^{3-}$ seen from the top and side.

competency and high activity for catalysis of a representative gas-phase reaction.

Briefly, POMs constitute a large class of polynuclear oxo-bridged early transition-metal compounds with a rich topology and versatile chemical and physical properties.[11] They are based on the assemblage of MO_n (M = addenda atoms e.g., W^{VI}, Mo^{VI}, V^{V}, Ti^{IV}, Nb^{V}, Ta^{V}) polyhedra, most commonly octahedra, interconnected via corner and edge sharing. Prominent subsets include Keggin $[XM_{12}O_{40}]^{n-}$ (10Å),[12] Dawson $[X_2M_{18}O_{62}]^{n-}$ (12Å),[13] and Anderson $[XM_6O_{24}]^{n-}$ (8.5Å)[14,15] type POMs. Anderson polyoxoanions are composed of six edge-sharing MoO_6 or WO_6 octahedra surrounding a central, edge-sharing heteroatom of octahedral geometry (XO_6) defining a planar arrangement having approximate D_{3d} symmetry. Three modes of oxygen anion coordination are found in the structure: 1) six triple-bridged oxygen atoms (μ_3-O) connect the heteroatom and two addenda atoms, 2) six double-bridged oxygen atoms (μ_2-O) connect two addenda atoms, and 3) two terminal oxygen atoms (O_t) are connected to each of the six addenda atoms. The general formula can be written as $[H_y(XO_6)M_6O_{18}]^{n-}$, where y=0-6, n=2-8, M=addenda atoms (Mo^{VI} or W^{VI}), and X=central heteroatom. The heteroatom can be any of several transition metals (Cr, Mn, Fe, Co, Ni, Cu, Zn, Pt, etc.) as well as certain main-group atoms (Te, I, Sb, etc.).[16] The combination of adjustable structure, and manifold compositions, has enabled polyoxometalates to contribute solutions to a great variety of chemical problems, but most notably catalysis,[17,18] including water oxidation,[19,20] alkene epoxidation,[21-23] and aldehyde[24] and/or alcohol oxidation.[25] Nevertheless, pure Anderson POMs typically offer limited active-site accessibility due to low surface area (<10 m^2/g),[26] low melting points, and difficulties for separation in solution-phase reactions, thus limiting their catalytic utility.

To overcome these limitations, porous supports such as mesoporous silica,[27,28] organic polymers,[29,30] covalent organic frameworks (COFs),[31] and metal-organic frameworks (MOFs)[32-34] have been used to anchor POMs and/or form hybrid heterogeneous materials. MOFs are porous crystalline materials consisting of metal-ion-containing nodes and multitopic organic linkers.[35,36] The tunability, crystalline periodicity, and porosity of MOFs make them promising both as heterogeneous catalysts[37] and as well-defined supports for subsequently introduced catalysts.[38,39] Zr-based MOFs, in particular, hold great potential for applications involving gas-phase catalysis due to their extraordinary thermal and chemical stabilities, as well as their substantial internal surface areas.[40] Suitable aperture and cavity sizes are key to confining and isolating individual POMs. Isolating POMs from each other via organic spacers could preclude unwanted POM migration and sintering, a common mode of deactivation of supported heterogeneous catalysts, especially at elevated temperature.

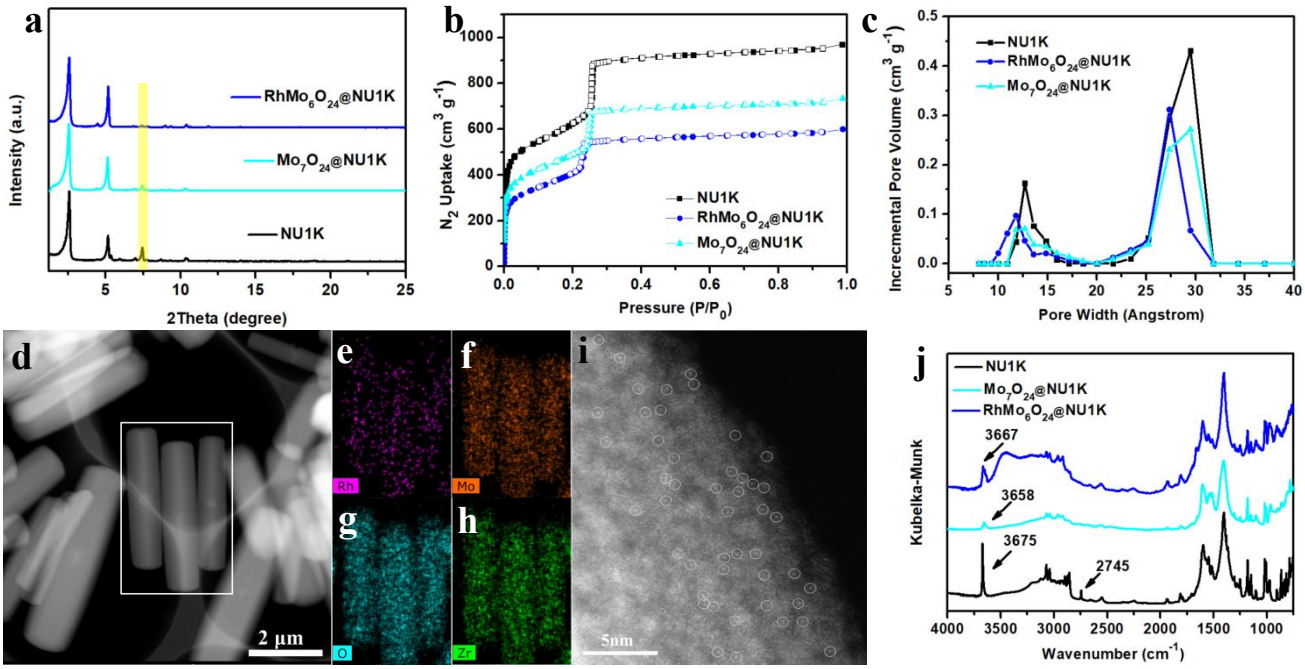

Figure 2. (a) PXRD patterns for NU1K, Mo_7O_{24}@NU1K and $RhMo_6O_{24}$@NU1K. (b) and (c) are N_2 isotherm and pore size distribution of NU1K, Mo_7O_{24}@NU1K and $RhMo_6O_{24}$@NU1K. (d) TEM images show that the size and morphology of NU1K crystallites are well maintained by $RhMo_6O_{24}$ installation. (e-h) EDS mapping suggests uniform distribution of $RhMo_6O_{24}$ clusters within NU1K crystallites. (i) HAADF-STEM image of $RhMo_6O_{24}$@NU1K clearly displays the Rh single atoms (highlighted by white circles) randomly dispersed on the NU1K. (j) DRIFT spectra of the NU1K, Mo_7O_{24}@NU1K and $RhMo_6O_{24}$@NU1K. Vibrational spectra recorded at 125 °C overnight in Argon.

Thus, we selected the hierarchically porous framework NU1K (Figure 1a). Featuring csq topology, it ideally comprises $Zr_6(\mu_3\text{-}O)_4(\mu_3\text{-}OH)_4(H_2O)_4(OH)_4^{8+}$ nodes[41-43] and tetratopic 1,3,6,8-(p-benzoate)pyrene ($TBAPy^{4-}$) linker that define 1D hexagonal and triangular channels of diameters ~31 Å and ~12 Å, respectively, with node-bounded cavities of diameter ~10 Å (denoted as *c*-pores) interconnecting the channels. Linkers occupy eight of twelve potential carboxylate-compatible node-binding sites, leaving four displaceable, nonstructural aqua/hydroxo ligand pairs. These ligands are oriented toward both hexagonal pores and/or *c*-pores, with the latter orientation being potentially useful for forming Zr-O(H)-POM linkages and immobilizing size-matched Anderson clusters.

Herein, we report our investigations on CO oxidation, catalyzed by $RhMo_6O_{24}$@NU1K, as a proof-of-concept reaction to demonstrate that spatial confinement of guests inside nanoporous hosts affords an effective strategy for obtaining and stabilizing reactant-accessible and uniformly sited single-metal-atom catalysts, particularly when the guest itself comprises a structurally well-defined, nanometer scale support for the catalytic atom. We prepared $(NH_4)_3[H_6RhMo_6O_{24}]\cdot 6H_2O$ (abbreviated as $RhMo_6O_{24}$) using $(NH_4)_6[Mo_7O_{24}]\cdot 4H_2O$ (Mo_7O_{24}) as a template, followed by confinement of $RhMo_6O_{24}$ in the *c*-pore of NU1K via solution-based impregnation. Synchrotron-based X-ray scattering methods, together with other spectroscopic methods, were used to establish the framework siting and corroborate the structure of the catalyst and its support. Competency for CO oxidation, a commonly used model reaction for single-atom catalysts, was then assessed. Diffuse reflectance infrared Fourier transform spectroscopy (DRIFTS) was adopted to probe the interaction of CO with single Rh atoms, with the results providing insights into the basis for catalytic activity.

Results and discussion

An example isomer of the standard Anderson POM structure is β-heptamolybdate (β-Mo_7O_{24}), which features "bent" rather than planar structure (Figure 1b).[44] β-Heptamolybdate can be viewed as three edge-shared octahedra in line with two octahedra located on each side of the space between the three octahedra. The two octahedra on each side are shifted by a half octahedron resulting in the "bent" structure (Figure 1b bottom). The average dimensions of the Mo_7O_{24} cluster are 9.32Å×8.6Å×5.65Å. Pale-yellow rhombic crystals of $(NH_4)_3[H_6RhMo_6O_{24}]\cdot 6H_2O$ were obtained from a mixed aqueous solution containing $Rh(NO_3)\cdot H_2O$ and $(NH)_6Mo_7O_{24}\cdot 4H_2O$. Substitution of Rh(III) for the central Mo of Mo_7O_{24} yields $RhMo_6O_{24}$ (Figure S1). As depicted in Figure 1c, planar $RhMo_6O_{24}$ consists of a {RhO_6} octahedron connected to six {MoO_6} octahedra in edge-sharing fashion. Based on single-crystal X-ray diffraction data (Table S1), this construct is characterized by a range of Rh-O bonds of varying (differing) lengths of 2.005-2.020 Å. The average dimensions of the overall cluster are *ca.* 8.55 Å×8.55 Å×3.15 Å.[45]

Due to the presence of large channels in NU1K, the direct impregnation was used to install $RhMo_6O_{24}$ and Mo_7O_{24}. To synthesize POM@NU1K compounds, powder NU1K was added and suspended in an aqueous POM solution at room

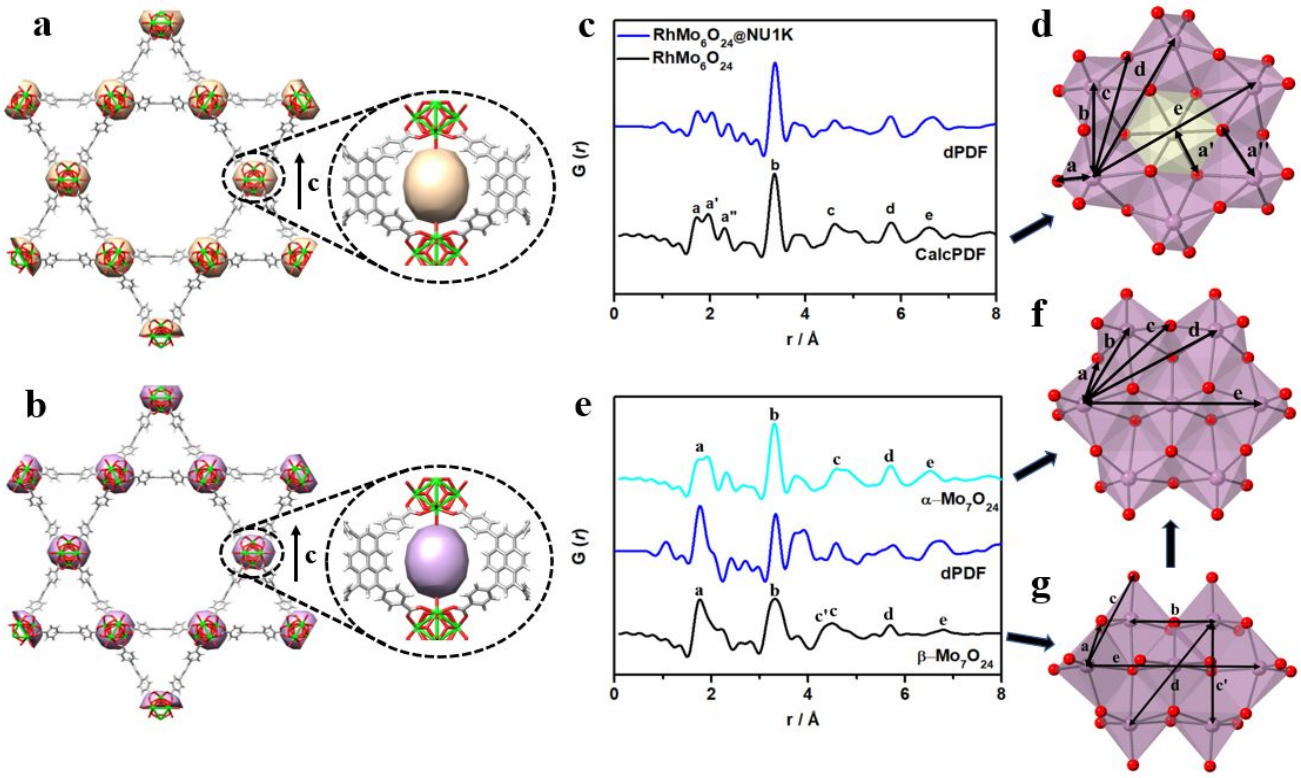

Figure 3. DEDs corresponding to the location of (a) $RhMo_6O_{24}$@NU1K (golden surface) and (b) Mo_7O_{24}@NU1K (purple surface) in electron density viewed parallel to the c-axis. Differential PDFs and polyhedral structures of (c, d) $RhMo_6O_{24}$@NU1K and (e-g) Mo_7O_{24}@NU1K obtained by subtraction of the PDF for pristine NU1K.

temperature. After 3 days, the solid was washed and rigorously solvent-exchanged with acetone, resulting in permanently porous, solvent-evacuated, hybrid materials after thermal treatment under vacuum. Details of the synthesis and activation of Mo_7O_{24}@NU1K and $RhMo_6O_{24}$@NU1K are discussed in the Experimental Section. Their unit cells, as seen by the Bragg peak positions on powder X-ray diffraction (Figure 2a), resemble that of NU1K, except for a decrease of the intensity of diffraction peaks at 2θ = 7.44° corresponding to a decrease in the coherency of planes with a spacing of 1.0 nm, highlighted in yellow. The diffraction pattern matches well with a predicted/simulated pattern where the POM is located between two nodes in the MOF *c*-pore.[46]

Consistent with POM incorporation, BET surface areas from experimental N_2 isotherms of $RhMo_6O_{24}$@NU1K and Mo_7O_{24}@NU1K decrease to 1330 and 1640 m^2/g, from 2170 m^2/g for vacant NU1K (Figure 2b). Similar to that of NU1K, the isotherms of $RhMo_6O_{24}$@NU1K and Mo_7O_{24}@NU1K show a type-IV feature-a step near $P/P_0 = 0.23$ -which is associated with the mesoporosity. The pore size distributions (PSDs) for $RhMo_6O_{24}$@NU1K and Mo_7O_{24}@NU1K both indicate a decrease in the width of the hexagonal pores to 27 Å compared to ~30 Å for POM-free NU1K, and for the trigonal pores a shrinkage 13 to 11 Å (Figure 2c). While the chemical basis for pore contraction is not clear, it has been observed previously when metal ions were deposited solvothermally in the *c*-pore of NU1K[47] and when aqua ligands were thermally removed from the nodes of formate-free NU1K-FF-Cl.[43] TEM images show that the size and morphology of NU1K crystallites are well unperturbed by $RhMo_6O_{24}$ installation (Figure 2d). EDS mapping suggests uniform distribution of $RhMo_6O_{24}$ clusters and, separately, Mo_7O_{24} clusters, within NU1K crystallites (Figure 2e-h, Figure S2 and Figure S3). To identify the form of the Rh atoms distributed in c-pore of NU1K, high-angle annular dark-field scanning transmission electron microscopy (HAADF-STEM) was used. It is shown in Fig. 2i that isolated Rh atoms were observed all over the support with no obvious nanoparticles or clusters present.

Initially present, node-sited formate ions are removed almost completely by POM installation, *i.e.*, only 0.38 formate per node remained following installation of Mo_7O_{24}, and only 0.13 formate per node following installation of $RhMo_6O_{24}$, compared with 3.0 ± 0.2 formate ligands (of a possible maximum of 4) per Zr_6 node of NU1K (Figure S4), based on solution-phase ^1H NMR spectra obtained by digesting samples in $NaOD/D_2O$. For POM@NU-1K, after 125°C heating in Ar overnight to remove physisorbed water, the sharp peak of NU1K at ~3675 cm^{-1} in the DRIFT spectrum is replaced with a broad peak at 3658 cm^{-1} for Mo_7O_{24}@NU1K and at 3667 cm^{-1} for $RhMo_6O_{24}$@NU1K, while the formate-associated peak at 2745 cm^{-1} disappears with installation of either POM (Figure 2j).[43] Formate anions are evidently displaced by anionic Anderson POMs. ICP-OES measurements indicate molar ratio of *ca.* 6:1 for Mo to Rh, consistent with the chemical composition of $RhMo_6O_{24}$. For $[H_6RhMo_6O_{24}]^{3-}$, the maximum loading after thorough washing, is 1.08 per Zr_6 node (or essentially one for each c-pore; see below). The maximum loading of $[Mo_7O_{24}]^{6-}$ is slightly lower:

0.67 per Zr_6 node. XPS (X-ray photoelectron spectroscopy) measurements reveal that the oxidation state for neither Rh nor Mo is altered. N 1s XPS spectra, NH_4^+ counter-ions are converted to NH_3 probably due to pH change, after encapsulation and subsequent washing steps. (Figure S5).[48]

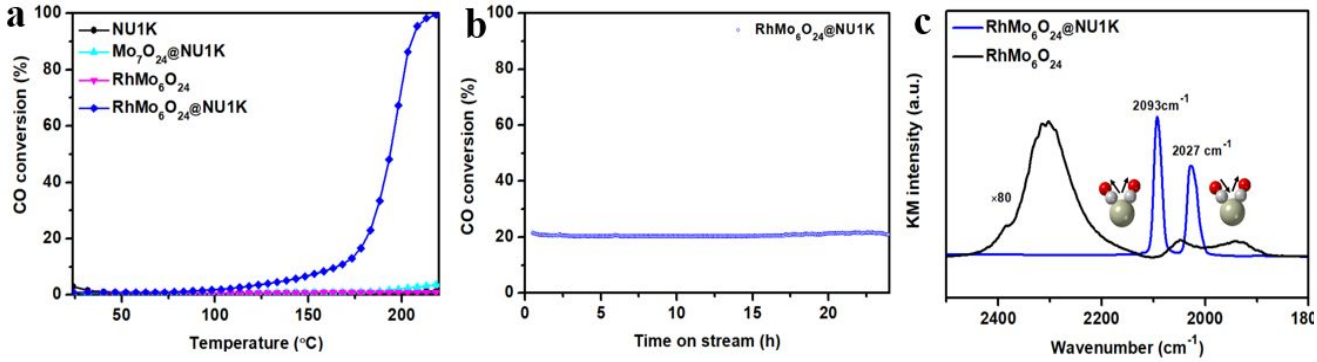

Figure 4. CO oxidation performance. (a) CO conversion profiles over NU1K, $RhMo_6O_{24}$, Mo_7O_{24}@NU1K and $RhMo_6O_{24}$@NU1K catalysts. (b) Stability test using $RhMo_6O_{24}$@NU1K at 180 °C. (c) DRIFT spectra of CO adsorption on the $RhMo_6O_{24}$ and $RhMo_6O_{24}$@NU1K catalysts at room temperature. Spectra were collected after CO adsorption to saturation and Ar purging.

To pinpoint the siting of the POMs, difference envelope density (DED) analyses of synchrotron-based X-ray scattering data were employed. This technique generates a surface envelope between regions of high and low electron density which can be extracted from low order, intense, independent reflections in a high-resolution PXRD pattern. Using differential analysis with a parent framework can yield a coarse map of electron density attributable to the incorporation of guest molecules.[49] DED analyses of $RhMo_6O_{24}$@NU1K and Mo_7O_{24}@NU1K reveal the localization of electron density exclusively within the MOF *c*-pore; see Figure 3, panels a and b. In the PDF (pair-distribution function) analysis of X-ray total-scattering data for pristine NU1K (Figure S6), sharp peaks at 1.4, 2.0, 3.5 and 5.0 Å are associated with C-C, Zr-O, Zr…Zr and Zr……Zr distances. Peaks at high r and oscillation are indicative of long-range order (as one would expect, for a crystalline material). The local and long-range order of the framework are well preserved as most of these features are also observed in PDF plots for POM-loaded samples. In the PDFs of POM-loaded samples, a peak indictive of the Mo-O bond length occurs at 1.7 Å. With $RhMo_6O_{24}$ installation in NU1K, the peak at 2.0 Å acquires a shoulder around 2.4 Å. A peak at 3.5 Å broadens and shifts to lower r, with more peaks growing and overlapping at higher r. With Mo_7O_{24} incorporation, other than the Mo-O peak growth, changes are too subtle to be observed.

To better understand the structure of the cluster when sited in the MOF, as well as the cluster's possible chemical interaction with the MOF, difference PDF (dPDF) data were acquired by scaling and subtracting the PDF of pristine NU1K from that for POM-loaded NU1K samples. The structure of $RhMo_6O_{24}$ in the NU1K is clear, as the dPDF of $RhMo_6O_{24}$@NU1K matches well with the $RhMo_6O_{24}$ structure in the notable peaks at 1.7 (a), 2.0 (a') and 2.4 Å (a'') corresponding to the Mo-O bond, and peaks at 3.3 (b), 5.8 (d) and 6.7 Å (e) related to the Mo-Mo/Rh distances (Figure 3c and 3d). In the dPDF of Mo_7O_{24}@NU1K (Figure 3e), sharp peaks are evident at 1.8 Å (a) and 3.3 Å (b). These correspond to the Mo-O bond length and the shortest Mo…Mo separation distance in edge-sharing Mo-O polyhedral-findings that are nominally consistent with the known single-crystal X-ray structure of "bent" Mo_7O_{24} (Figure 3g).[50] The large peak at 3.8 Å in the dPDF plot is likely related to the interaction between the framework and the POM, *i.e.* Zr…Mo.[49] The peak can be speculatively rationalized based on Zr(IV)-O(H)-Mo(VI) linkages, *i.e.* chemical grafting of the POM to nodes. Interestingly, dPDF peak locations at higher r differ from those expected for indicates the connection between these polyhedra is not the same as the "bent" structure. β-Mo_7O_{24}, with a boat-like configuration, has a greater variety of Mo…Mo distance than does the planar α-Mo_7O_{24} configuration. Comparison of calculated dPDF plots for these two to the experimental plot for $RhMo_6O_{24}$@NU1K reveals closer agreement of $RhMo_6O_{24}$@NU1K with α-Mo_7O_{24} (Figure 3f). We note, in particular, the absence vs. presence of a Mo…Mo peak at 4.2 Å (c') that is unique to β-Mo_7O_{24}, was found related to the Mo…Mo distance in the model. The combined results suggest that Mo_7O_{24} siting in NU1K is accompanied by isomerization of the "bent" β to the "planar" α form.

CO oxidation by dioxygen to carbon dioxide is a classic model reaction for heterogeneous catalysis. Here CO oxidation was evaluated in a fixed-bed flow reactor with a reaction gas of 0.5 vol% CO + 20 vol% O_2 and He balance. Pure $RhMo_6O_{24}$ barely registers catalytic activity in measurements up to 220°C. In contrast, samples of $RhMo_6O_{24}$@NU1K, despite offering much lower Rh content, show a light-off temperature (the temperature at which CO conversion reaches 10%) of 120°C and a T_{100} (the temperature for 100% CO conversion) of 220°C, evincing both its high activity and the salutary effects of MOF-based nano-confinement. The activation energy for the reaction is extracted from the Arrhenius plot and estimated as 55 kJ mol^{-1} (Figure S7). Control experiments established that rhodium-free Mo_7O_{24}@NU1K is inactive at temperatures below 200°C,

implying that the extremely high activity of $RhMo_6O_{24}$@NU1K originates either from the single Rh atoms or from the cooperation of the Rh atom and the localized molybdenum-oxide support (Figure 4a). For practical use, long-term stability obviously is crucial. We, therefore, tested the stability of $RhMo_6O_{24}$@NU1K at 180°C. The initial conversion was controlled below 100% to avoid activity saturation. The material remains a free-flowing powder after catalysis, showing no signs of sintering on stream. This reactivity profile is maintained throughout a 24 h stability test (Figure 4b), indicating negligible catalyst deactivation. $RhMo_6O_{24}$ and $RhMo_6O_{24}$@NU1K were further monitored by *in situ* DRIFTS following CO exposure, because this technique is reliable for assessing rhodium atom accessibility and for differentiating between single rhodium atoms and rhodium clusters. After 10 min of exposure to CO, followed by 10 min of argon purging, stable DRIFT spectra were obtained. For $RhMo_6O_{24}$@NU1K, exposure yields prominent peaks at approximately 2093 and 2027 cm^{-1}, attributable to symmetric and asymmetric vibrations, respectively, of gem-dicarbonyl Rh(I) (Figure 4c).[51] These values are also in line with the computed IR frequencies of a Rh(I) gem-dicarbonyl POM (see supporting information for the computational study details, Figure S8-9 and Table S2-3). In contrast, nonporous, low-surface-area $RhMo_6O_{24}$ registers almost no response to CO and, in particular, no obvious response indication of gem-dicarbonyl species.

Returning to the MOF-confined Rh species, as the temperature increases from 40 to 130°C, the intensities of the gem-dicarbonyl rhodium peaks decrease slightly, implying slight desorption. Exposure to O_2 at 150°C yields slightly larger decreases. Notably, however, peaks due to bridged CO (1860 cm^{-1}) or linear CO on Rh^0 (2070 cm^{-1}) are absent (Figure S10)-thus ruling out the formation of Rh clusters and indicating the preservation of the catalyst in single-rhodium-atom form.[52] DED analysis of $RhMo_6O_{24}$@NU1K after catalysis reveals that POM is still in c-pore (Figure S11).The dPDF of $RhMo_6O_{24}$@NU1K after catalysis is similar to that of fresh sample(Figure S12), indicating that no migration and agglomeration of isolated cluster happened during reaction. Post-catalytic characterization of $RhMo_6O_{24}$@NU1K samples yielded PXRD patterns that align well with the as-synthesized materials, shown in Figure S13. In addition, N_2 isotherm analysis shows a slight drop in porosity, with the drop occurring mainly in the material's mesopores of these (Figure S14). This can be attributed to a combination of partial pore collapse and residual low surface area support materials from the reactor bed (SiO_2 and quartz wool). This phenomenon is consistent with the post-catalytic of NU1K and other MOFs.[53] XAFS fitting data before and after catalysis were used to demonstrate consistency of bond lengths and coordination numbers of isolated $RhMo_6O_{24}$ cluster (Figure S15-17 and Table S4-6).

A systematic investigation of the mechanism of single-rhodium-atom-catalyzed ($RhMo_6O_{24}$@NU1K-catalyzed) oxidation of CO by O_2 is beyond the scope of this study. Nevertheless, we note that: a) $RhMo_6O_{24}$ as initially formulated features coordinative saturation of Rh(III) by bridging oxo anions, b) exposure of $RhMo_6O_{24}$@NU1K to CO, a potential reductant, is accompanied by conversion of Rh(III) to Rh(I) and by coordination of two carbonyls, and c) gem-dicarbonyl rhodium(I) formation implies loss of two core oxo ligands from the cluster, and suggests formation of oxygen vacancies proximal to the single rhodium atom. Thus, an important feature of the cluster-based oxy-Mo(VI) support may be to stabilize vacancies. In turn, the apparent presence of proximal vacancies suggests O_2 activation and CO oxidation, at least in part, by a Mars-van Krevelen or similar mechanism, *i.e.* a mechanism entailing transfer of a lattice (cluster) oxygen atom to CO to yield CO_2, presumably with cycling between single-rhodium-atom oxidation states III and I.

Conclusions

We find that stabilization of single rhodium atoms by isolation in molybdenum-based Anderson POMs, followed by spontaneous installation and grafting of the POMs within sized-matched pores of NU1K serves to spatially isolate the rhodium atoms. Loading is quantitative and isolation persists even with prolonged heating and time-on-line as catalysts. DED and PDF analyses of scattering of synchrotron-generated X-rays pinpoint the location of the POM and establishes that it is oriented such that the planar, hexa-molybdenate cluster, rather than the MOF node, serves as the support for the isolated rhodium atom. Exposure to CO establishes that: a) the MOF-confined and POM-confined Rh atoms are easily accessed by gas-phase molecules, b) each Rh center can bind two carbonyls, c) the oxidation state of the rhodium atom is reduced from III to I, d) two (or more) bridging oxo ligands are shed by the rhodium atom, but e) evolution of the coordination environment does not lead to rhodium atom clustering, loss or agglomeration. Simultaneous exposure of the confined single-rhodium-atoms to CO and O_2 leads to rapid and sustained catalytic conversion of CO to CO_2 at modest temperatures. In striking contrast, pure, MOF-free $(NH_4)_3RhMo_6O_{24}{\cdot}6H_2O$, a nonporous compound, displays almost no interaction with CO and exhibits little or no detectable catalytic activity even at 220°C, the highest temperature examined. The contrast underscores the effectiveness of MOF/Anderson-POM ensembles for presenting stable, uniform, reactant-accessible arrays of single-atom catalysts. Given the large number of central-metal variants of Anderson POMs and their close size-matching with the *c*-pore of the platform MOF, NU1K, we suggest that many more opportunities exist for similarly presenting stable arrays of single-metal-atom catalysts, including arrays presenting combinations of single-metal-atom catalysts that may be suitable for cascade catalysis.

Experimental Details

Synthesis of $(NH_4)_3[H_6RhMo_6O_{24}]{\cdot}6H_2O$: Pale-yellow rhombic crystals were obtained from a mixed aqueous solution containing $Rh(NO_3){\cdot}H_2O$ and $(NH_4)_6Mo_7O_{24}{\cdot}4H_2O$ (Mo_7O_{24}), modified according to the literature.[45] The Rh replaced the central Mo of $(NH_4)_6Mo_7O_{24}{\cdot}4H_2O$ to form $(NH_4)_3[H_6RhMo_6O_{24}]{\cdot}6H_2O$

Synthesis of $RhMo_6O_{24}$@NU1K: In a centrifuge tube, $RhMo_6O_{24}$ (60 mg, 0.023 mol) was dissolved in 10 mL of deionized water. To solution, NU1K (50 mg, 0.023 mmol) was added and suspended by sonicating for about 1 min. The suspension was shaken periodically. To monitor uptake of POM, the solutions with and without NU1K were analyzed by ICP-OES and compared to each other. After 3 days, the solid was washed with water three times. Then, the solid was washed with acetone. $RhMo_6O_{24}$@NU1K was allowed to soak in acetone overnight before being washed two more times with acetone to ensure adequate removal of water. Samples were dried at 80°C for 4 h under a vacuum prior to activation on the Smart VacPrep. The solid material was subject to ICP-OES to determine the final POM loading. Synthesis of Mo_7O_{24}@NU1K is similar to that of $RhMo_6O_{24}$@NU1K using commercial Mo_7O_{24}.

Catalysis with gas-phase reactants: The catalyst evaluation was performed using a modified, Altamira BenchCAT4000 reactor system housed in the Reactor Engineering and Catalyst Testing (REACT) core facility at Northwestern University. The reagent gases were supplied using a 0.5% CO, 20% O_2 balanced with He mixture (AirGas). The POM content of all catalysts is unified to 5mg diluted with 1.5 g of low surface area, white quartz sand (Sigma-Aldrich, ≥99.995% trace metals basis) and packed in a quartz tube. The catalyst temperature was controlled with a K-type thermocouple at the top of the catalyst bed. For Figure 4a, the catalytic performance was investigated by temperature-programmed heating with rate of 1 °C ·min^{-1} with mixed gas at a flow rate of 10 mL/min. For Figure 4b, the reactions were kept at a specific temperature for 24 h. The gas products were analyzed with an on-line Agilent 7890A GC, equipped with a HP-PlotQ column and a FID detector. The FID detector utilized an Advanced Research Company Jetanizer methanizing unit for the detection of CO and CO_2.

DRIFTS experiments: In situ diffuse reflectance infrared Fourier transform (DRIFT) spectra experiments were carried out by using a Thermo-Nicolet iS50 FTIR spectrometer, and Harrick Scientific's Praying Mantis DRIFTS accessory and heating reaction chamber. For the DRIFTS experiments, neat samples ($RhMo_6O_{24}$ and $RhMo_6O_{24}$@NU1K) were crashed by using mortar and pestle, and placed in the sample cup of the DRIFT reaction chamber. During the test, the gas pressure is atmospheric pressure. Then, temperature was raised to the setpoint (190°C) under H_2 in balance Ar flowing at about 30 mL/min; and kept isothermal for the removal of physisorbed water and the reduction of sample. This process was monitored by FTIR; a background spectrum was taken when temperature reached at a given setpoint, and used as reference for the subsequent spectra. IR spectra were acquired for the course of 30-45 min until spectral changes in the OH stretch region are negligible. The gas was switched to neat Ar flowing at 30 ml/min. Then, sample was cooled down to 40°C with 20°C temperature intervals while a background spectrum was collected at each point. Next, sample was treated with 5% CO in balance Ar flowing at about 30 mL/min. IR spectra were continuously acquired during this dosing step. When the main CO band at about 2050 cm^{-1} was plateaued the flow was switched to pure Ar. This purging step was carried out for about 15 min until the gas phase CO peak disappeared and the main metal-CO band is not changing. A spectrum was recorded at the end of this step. The chamber temperature was then increased, and a sample spectrum was acquired by using the reference spectrum taken prior at the designated temperature. After the spectrum in Ar atmosphere at 130°C was acquired, the chamber was cooled to 70°C at which a final spectrum in Ar was collected. Next, the gas was switched to 10% O_2 in balance Ar, and sample spectra were taken in the 70-150°C range with 20°C intervals.

Author Contributions

J.T.H. and Q.L. supervised the project and designed the experiments. Q.L. carried out most of the experiments and analysed the data. Z.C. and K.W.C. carried out DED and PDF characterizations. H.S. and R.B.G. carried out computational modeling. N.S. and S.A. conducted CO-DRIFT spectrum experiments. J.D., W.B., Z.L., S.G., Q.W., and J.M.N. carried out partial experimental characterizations. Q.L. and J.T.H. cowrote the paper. All authors discussed the results

Conflicts of interest

There are no conflicts of interest to declare.

Acknowledgements

J. T. H. thanks Prof. Bruce Gates for useful discussions. This work was supported as part of the Inorganometallic Catalyst Design Center, an EFRC funded by the DOE, Office of Science, Basic Energy Sciences (DE-SC0012702). Q. L. thanks Weiren Chen for EXAFS fitting. Q. L. acknowledge the financial support from the National Natural Science Foundation of China (No. 11705205). W. B. acknowledge the financial support from the Natural Science Foundation of China (No. U1832168, 22175051), the Anhui Provincial Natural Science Foundation (No. 1808085MB26). Z. L. gratefully acknowledges support from the National Natural Science Foundation of China (21601047), the Fundamental Research Funds for the Central Universities (2018B17614), and the China Scholarship Council (CSC) (201806715039) during his visit to Northwestern University. This work made use of the J.B. Cohen X-ray Diffraction Facility supported by the IMRSEC program of the National Science Foundation (DMR-1121262) at the Materials Research Center of Northwestern University. This work made use of the Reactor Engineering and Catalyst Testing (REACT) core facility of the Center for Catalysis and Surface Science at Northwestern University. This work made use of the EPIC and Keck-II facilities of the NUANCE Center at Northwestern University, which has received support from the Soft and Hybrid Nanotechnology Experimental (SHyNE) Resource (NSF ECCS-1542205); the MRSEC program (NSF DMR-1720139) at the Materials Research Center; the International Institute for Nanotechnology (IIN); the Keck Foundation; and the State of Illinois, through the IIN. Use

of the Advanced Photon Source is supported by the U.S. Department of Energy, Office of Science, and Office of Basic Energy Sciences, under Contract DE-AC02-06CH11357. Materials Research Collaborative Access Team (MRCAT, Sector 5-BM) operations are supported by the Department of Energy and the MRCAT member institutions. The REACT Core facility acknowledges funding from the U.S. Department of Energy, Office of Science, Office of Basic Energy Sciences, Catalysis Science program (DE-SC0001329) used for the purchase of the Altamira BenchCAT4000 reactor system and Agilent 7890 GC and the U.S. Department of Energy, Office of Science, Office of Basic Energy Sciences, Catalysis Science program (DE-FG02-03ER15457) used for the purchase of the Nicolet 6700 FT.

Notes and references

(1) Kaiser, S. K.; Chen, Z.; Akl, D. F.; Mitchell, S.; Ramírez, J. P. Single-Atom Catalysts across the Periodic Table. *Chem. Rev.* **2020,** *120,* 11703-11809.

(2) Basic Research Needs for Catalysis Science. United States: N. p., 2017. Web. doi:10.2172/1545774.

(3) Hannagan, T. R.; Giannakakis, G.; Stephanopoulos, F. M.; Sykes.; C. H. E. Single-Atom Alloy Catalysis. *Chem. Rev.* **2020,** *120,* 12044-12088.

(4) Ji, S.; Chen, Y.; Wang, X.; Zhang, Z.; Wang, D.; Li.; Y. Chemical Synthesis of Single Atomic Site Catalysts. *Chem. Rev.* **2020,** *120,* 11900-11955.

(5) Feng, L.; Day, S. G.; Wang, K. Y.; Yuan, S.; Zhou, H. C. Strategies for Pore Engineering in Zirconium Metal-Organic Frameworks. *Chem* **2020,** *6,* 2902-292.

(6) Kim, S. I.; Ahn, S.; Vermeulen, A. N.; Webber, E. T.; Gallington, C.L.; Chapman, W. K.; Penn, L. R.; Hupp, T. J.; Farha, K. O.; Notestein, M. J.; Martinson, B. F. A. The Synthesis Science of Targeted Vapor-Phase Metal-Organic Framework Postmodification. *J. Am. Chem. Soc.* **2020,** *142,* 242-250.

(7) Islamoglu, T.; Goswami, S.; Li, Z.; Howarth, J. A.; Farha, K. O.; Hupp. T. J. Postsynthetic Tuning of Metal-Organic Frameworks for Targeted Applications. *Acc. Chem. Res.* **2017,** *50,* 805-813.

(8) Babucci, M.; Guntida, A.; Gates, C. B. Atomically Dispersed Metals on Well-Defined Supports including Zeolites and Metal-Organic Frameworks: Structure, Bonding, Reactivity, and Catalysis. *Chem. Rev.* **2020,** *120,* 11956-11985.

(9) Rogge, S. M. J.; Bavykina, A.; Hajek, J.; Garcia, H.; Olivos-Suarez, A. I.; Sepúlveda-Escribano, A.; Vimont, A.; Clet, G.; Bazin, P.; Kapteijn, F.; Daturi, M.; Ramos-Fernandez, E. V.; Llabrés i Xamena, F. X.; Speybroeck, V. Van.; Gascon; J. Metal-organic and covalent organic frameworks as single-site catalysts. *Chem. Soc. Rev.,* **2017,** *46,* 3134-3184.

(10) Long, L. D.; Tsunashima, R.; Cronin, L. Polyoxometalates: Building Blocks for Functional Nanoscale Systems. *Angew. Chem. Int. Ed.* **2010,** *49,* 1736-1758.

(11) Pope, M. Heteropoly and Isopoly Oxometalates. Springer-Verlag, Berlin, **1983.**

(12) Keggin, F. J. Structure of the Crystals of 12-Phosphotungstic Acid. *Nature* **1933,** *132,* 351.

(13) Dawson, B. The structure of the 9(18)-heteropoly anion in potassium 9(18)-tungstophosphate, $K_6(P_2W_{18}O_{62})\cdot 14H_2O$. *Acta Cryst.* **1953,** *6,* 113-126.

(14) Anderson, J. S. Constitution of the Poly-acids. *Nature* **1937,** *140,* 850.

(15) Evans Jr., T. H. The Crystal Structures of Ammonium and Potassium Molybdotellurates. *J. Am. Chem. Soc.* **1948,** *70,* 1291-1292.

(16) Blazevic, A.; Rompel, A. The Anderson-Evans polyoxometalate: From inorganic building blocks via hybrid organic-inorganic structures to tomorrows "Bio-POM". *Coord. Chem. Rev.* **2016,** *307,* 42-64.

(17) Kozhevnikov, I. V. Catalysis by Heteropoly Acids and Multicomponent Polyoxometalates in Liquid-Phase Reactions. *Chem. Rev.* **1998,** *98,* 171.

(18) Long, D. L.; Tsunashima, R.; Cronin, L. Polyoxometalates: Building Blocks for Functional Nanoscale Systems. *Angew. Chem., Int. Ed.* **2010,** *49,* 1736

(19) Bloor, L. G.; Solarska, R.; Bienkowski, K.; Kulesza, P. J.; Augustynski, J.; Symes, M. D.; Cronin, L. Solar-driven water oxidation and decoupled hydrogen production mediated by an electron-coupled proton buffer. *J. Am. Chem. Soc.* **2016,** *138 (21),* 6707-6710.

(20) Li, N.; Liu, J.; Dong, B. X.; Lan, Y. Q. Polyoxometalate-Based Compounds for Photo- and Electrocatalytic Applications. *Angew. Chem. Int. Ed.* **2020,** *132,* 20963-20977.

(21) Lv, H.; Geletii, Y. V.; Zhao, C.; Vickers, J. W.; Zhu, G.; Luo, Z.; Song, J.; Lian, T.; Musaev, D. G.; Hill, C. L. Polyoxometalate water oxidation catalysts and the production of green fuel. *Chem. Soc. Rev.* **2012,** *41 (22),* 7572-7589.

(22) Mizuno, N.; Yamaguchi, K.; Kamata, K. Epoxidation of olefins with hydrogen peroxide catalyzed by polyoxometalates. *Coord. Chem. Rev.* **2005,** *249,* 1944-1956.

(23) Zhou, Z.; Dai, G.; Ru, S.; Yu, H.; Wei, Y. G. Highly selective and efficient olefin epoxidation with pure inorganic-ligand supported iron catalysts. *Dalton Trans.* **2019,** *48,* 14201-14205.

(24) Yu, H.; Ru, S.; Dai, G. Y.; Zhai, Y. Y.; Lin, H. L.; Han, S.; Wei, Y. G. An Efficient Iron(III)-Catalyzed Aerobic Oxidation of Aldehydes in Water for the Green Preparation of Carboxylic Acids. *Angew. Chem. Int. Ed.* **2017,** *56,* 3867-3871;

(25) Wang, Y.; Wu, Z.; Yu, H.; Han, S.; Wei, Y. G. Highly efficient oxidation of alcohols to carboxylic acids using a polyoxometalate-supported chromium(III) catalyst and CO_2. *Green Chem.* **2020,** 22, 3150-3154.

(26) Zhang, B.; Asakura, H.; Yan, N. Atomically Dispersed Rhodium on Self-Assembled Phosphotungstic Acid: Structural Features and Catalytic CO Oxidation Properties. *Ind. Eng. Chem. Res.* **2017,** 56, 3578-3587.

(27) Thompson, D. J.; Zhang, Y.; Ren, T. Polyoxometalate [γ-$SiW_{10}O_{34}(H_2O)_2]^{4-}$ on MCM-41 as catalysts for sulfide oxygenation with hydrogen peroxide. *J. Mol. Catal. A: Chem.* **2014,** *392,* 188-193.

(28) Fazaeli, R.; Aliyan, H.; Ahmadi, M. A.; Hashemian, S. Host (aluminum incorporated mesocellulous silica foam (Al-MCF))-guest (tungsten polyoxometalate) nanocomposite material: An efficient and reusable catalyst for selective oxidation of sulfides to sulfoxides and sulfones. *Catal. Commun.* **2012,** *29,* 48-52.

(29) Frenzel, R.; Morales, D.; Romanelli, G.; Sathicq, G.; Blanco, M.; Pizzio, L. Synthesis, characterization and catalytic evaluation of $H_3PW_{12}O_{40}$ included in acrylic acid/acrylamide polymer for the selective oxidation of sulfides. *J. Mol. Catal. A: Chem.* **2016,** *420,* 124-133.

(30) Miras, H. N.; Vila-Nadal, L.; Cronin, L. Polyoxometalate based open-frameworks (POM-OFs). *Chem. Soc. Rev.* **2014,** *43,* 5679-5699.

(31) Ma, H.; Liu, B.; Li, B.; Zhang, L.; Li, Y. G.; Tan, H. Q.; Zang, H. Y.; Zhu, G. Cationic Covalent Organic Frameworks: A Simple Platform of Anionic Exchange for Porosity Tuning and Proton Conduction. *J. Am. Chem. Soc.* **2016,** *138,* 5897-5903.

(32) Ferey, G.; Mellot-Draznieks, C.; Serre, C.; Millange, F.; Dutour, J.; Surble, S.; Margiolaki, I. A chromium terephthalate-based solid with unusually large pore volumes and surface area. *Science* **2005,** *309,* 2040-2042.

(33) Du, D.-Y.; Qin, J.-S.; Li, S.-L.; Su, Z.-M.; Lan, Y.-Q. Recent advances in porous polyoxometalate-based metal-organic framework materials. *Chem. Soc. Rev.* **2014,** *43,* 4615-4632.

(34) Ahn, S.; Nauert, L. S.; Buru, T. C.; Rimoldi, M.; Choi, H.; Schweitzer, M. N.; Hupp, T. J.; Farha, K. O.; Notestein, M. J.

Pushing the Limits on Metal-Organic Frameworks as a Catalyst Support: NU-1000 Supported Tungsten Catalysts for o-Xylene Isomerization and Disproportionation. *J. Am. Chem. Soc.* **2018,** *140,* 8535-8543.
(35) Howarth, A. J.; Peters, A. W.; Vermeulen, N. A.; Wang, T. C.; Hupp, J. T.; Farha, O. K. Best Practices for the Synthesis, Activation, and Characterization of Metal-Organic Frameworks. *Chem. Mater.* **2017,** *29*, 26-39.
(36) Zhou, H. C.; Long, J. R.; Yaghi, O. M. Introduction to metalorganic frameworks. *Chem. Rev.* **2012,** *112*, 673-674.
(37) Lee, J.; Farha, O. K.; Roberts, J.; Scheidt, K. A.; Nguyen, S. T.; Hupp, J. T. Metal-organic framework materials as catalysts. *Chem. Soc. Rev.* **2009,** *38*, 1450-1459.
(38) Wang, Z.; Cohen, S. M. Postsynthetic modification of metal-organic frameworks. *Chem. Soc. Rev.* **2009,** *38*, 1315-1329.
(39) Buru, T. C.; Farha, K. O. Strategies for Incorporating Catalytically Active Polyoxometalates in Metal-Organic Frameworks for Organic Transformations. *ACS Appl. Mater. Interfaces* **2020,** *12,* 5345-5360.
(40) Howarth, A. J.; Liu, Y.; Li, P.; Li, Z.; Wang, T. C.; Hupp, J. T.; Farha, O. K. Chemical, thermal and mechanical stabilities of metal-organic frameworks. *Nat Rev Mater* **2016**, *1,* 15018.
(41) Yang, D.; Bernales, V.; Islamoglu, T.; Farha, K. O.; Hupp, T. J.; Cramer, J. C.; Gagliardi, L.; Gates, C. B. Tuning the Surface Chemistry of Metal Organic Framework Nodes: Proton Topology of the Metal-Oxide-Like Zr_6 Nodes of UiO-66 and NU-1000. *J. Am. Chem. Soc.* **2016,** *138,* 15189-15196.
(42) Planas, N.; Mondloch, E. J.; Tussupbayev, S.; Borycz, J.; Gagliardi, L.; Hupp, T. J.; Farha, K. O.; Cramer, J. C. Defining the Proton Topology of the Zr_6-Based Metal-Organic Framework NU-1000. *J. Phys. Chem. Lett.* **2014,** *5,* 3716-3723.
(43) Lu, Z.; Liu, J.; Zhang, X.; Liao, Y.; Wang, R.; Zhang, K.; Lyu, J.; Farha, K. O.; Hupp, T. J. Node-Accessible Zirconium MOFs. *J. Am. Chem. Soc.* **2020,** *142,* 21110-21121.
(44) Lindqvist, I. Structure of the paramolybdate ion. *Acta Crystallogr.* **1950,** *3,* 159-160.
(45) Ozawa, Y. B.; Hayashi. Y,; Isobe, K. Structure of Triammonium Hexahydrogenhexamolybdorhodate(III) Hexahydrate. *Acta Cryst.* **1991,** *C47,* 637-638.
(46) Buru, T. C.; Li, P.; Mehdi, L. B.; Dohnalkova, A.; Prats, E. P. A.; Browning, D. N.; Chapman, W. K.; Hupp, T. J.; Farha, K. O. Adsorption of a Catalytically Accessible Polyoxometalate in a Mesoporous Channel-type Metal-Organic Framework. *Chem. Mater.* **2017,** *29,* 5174-5181.
(47) Noh, H.; Cui, Y.; Peters, A. W.; Pahls, D. R.; Ortuno, M. A.; Vermeulen, N. A.; Cramer, C. J.; Gagliardi, L.; Hupp, J. T.; Farha, O. K. An Exceptionally Stable Metal-Organic Framework Supported Molybdenum(VI) Oxide Catalyst for Cyclohexene Epoxidation. *J. Am. Chem. Soc.* **2016,** *138,* 14720-14726.
(48) Klet, C. R.; Liu, Y.; Wang, C. T.; Hupp, T. J.; Farha, K. O. Evaluation of Brønsted acidity and proton topology in Zr- and Hf-based metal-organic frameworks using potentiometric acid-base titration. *J. Mater. Chem. A*, **2016,** *4,* 1479-1485.
(49) Platero-Prats, A. E.; League, A. B.; Bernales, V.; Ye, J.; Gallington, L. C.; Vjunov, A.; Schweitzer, N. M.; Li, Z.; Zheng, J.; Mehdi, B. L.; Stevens, A. J.; Dohnalkova, A.; Balasubramanian, M.; Farha, O. K.; Hupp, J. T.; Browning, N. D.; Fulton, J. L.; Camaioni, D. M.; Lercher, J. A.; Truhlar, D. G.; Gagliardi, L.; Cramer, C. J.; Chapman, K. W. Bridging Zirconia Nodes within a Metal-Organic Framework via Catalytic Ni-Hydroxo Clusters to Form Heterobimetallic Nanowires. *J. Am. Chem. Soc.* **2017**, *139*, 10410-10418.
(50) Salts, P. T. Crystal Structure of the Heptamolybdate(vi) (Paramolybdate) Ion, [Mo,02,16-, in the Ammonium. *J.C.S. Dalt.* **1975**, No. vi, 505.
(51) Jeong, H.; Lee, G.; Kim, S. B.; Bae, J.; Han, W. J.; Lee, H.; Fully Dispersed Rh Ensemble Catalyst To Enhance Low-Temperature Activity. *J. Am. Chem. Soc.* **2018,** *140,* 9558-9565.
(52) Hülsey, J. M.; Zhang, B.; Ma, Z.; Asakura, H.; Do, A. D.; Chen, W.; Tanaka, T.; Zhang, P.; Wu, Z.; Yan, N. In situ spectroscopy-guided engineering of rhodium single-atom catalysts for CO oxidation. *Nat. Commun.* **2019,** *10,* 1330.
(53) Mian, R. M.; Redfern, R. L.; Pratik, M. S.; Ray, D.; Liu, J.; Idrees, B. K.; Islamoglu, T.; Gagliardi, L.; Farha, K. O. Precise Control of Cu Nanoparticle Size and Catalytic Activity through Pore Templating in Zr Metal-Organic Frameworks. *Chem. Mater.* **2020,** *32,* 3078-3086.